Fuzzy Logic vs. Classical PI Voltage Controller for a Self-Excited Induction Generator

MATEO BAŠIĆ, DINKO VUKADINOVIĆ, MILJENKO POLIĆ
Faculty of Electrical Engineering, Mechanical Engineering and Naval Architecture
University of Split
R. Boškovića 32, 21000 Split
CROATIA
mabasic@fesb.hr, dvukad@fesb.hr, miljenko.polic21@gmail.com

Abstract: - Vector control algorithms are often used for control of the self-excited induction generators (SEIGs). This paper presents a comparative analysis of two different approaches for control of the SEIG's generated voltage in a vector control system. The classical approach based on the PI control is first considered and then a fuzzy-logic-based alternative is proposed. In particular, two different-type fuzzy logic (FL) controllers, Mamdani and Sugeno, are developed for the purpose. The analysis and comparison of the controllers' performance is provided for step changes in load and DC voltage reference. The obtained simulation results are experimentally verified.

Key-Words: - Self-excited induction generator, Vector control, Dynamic analysis, PI controller, Fuzzy logic controller

1 Introduction

The capability of the squirrel-cage induction generator to excite without an external reactive power source was discovered in the 1930s [1], [2]. This capability allowed the application of squirrel-cage induction generators in stand-alone power generating systems, in which the reactive power from the grid is not available and which are usually associated with renewable energy sources [3]-[5]. Until recently, however, the widespread application of self-excited induction generators (SEIGs) was not possible due to the problems related with the instability of the generated voltage. Only with the advent of insulated-gate bipolar transistors (IGBTs) and microcontrollers these problems could be successfully overcome.

Vector control algorithms are today dominantly applied in SEIG control systems due to their superior control features. Most of such systems reported in literature employ classical PI controllers because of the simple design and satisfactory performance [5]-[7]. More advanced approaches based on fuzzy logic and artificial intelligence have also been considered [3], [8], but those are usually adopted for maximum power point tracking while the voltage control is almost exclusively handled by means of the PI controller.

In this paper, the advanced fuzzy-logic-based approach to SEIG voltage control is considered. Unlike the classical PI controller, the fuzzy logic (FL) controller does not require knowledge of a detailed mathematical model of the control system. Also, it has the capability of handling uncertain and noisy signals, and usually leads to better results compared to the conventional controllers, in terms of response time, settling time and robustness [9]. On the other hand, this is usually achieved at the expense of an increase in the computational requirements. It should also be noted that designing of the FL controller requires expert knowledge of the control system, and in the case of very complex systems it may prove to be very tedious or even impossible task. Therefore, the final decision about which type of voltage controller presents the best overall choice depends on various parameters. In this paper, two different-type FL controllers are developed for control of the SEIG voltage. Their application in the SEIG vector control system is proposed and overall performance evaluated by comparison with the optimally-tuned classical PI controller. The analysis is carried out both on the simulation and experimental level.

2 SEIG Vector Control System

Basic configuration of the SEIG vector control system under consideration is shown in Fig.1. As it can be seen, an indirect rotor-field-oriented (IRFO) algorithm is employed for control of the SEIG's generated voltage.

ISBN: 978-960-474-305-6

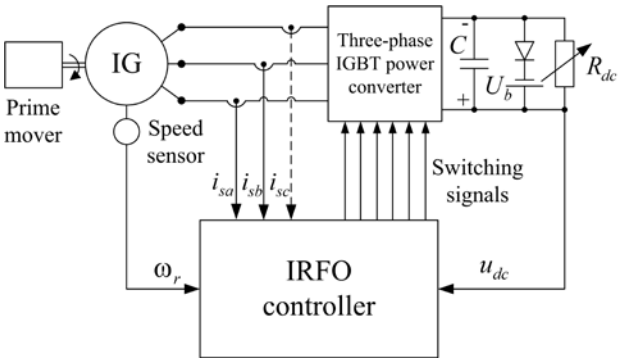

Fig.1 Basic configuration of the SEIG vector control system

The main components of the system are the induction generator, the prime mover, the IGBT converter, the IRFO controller and the DC link. The battery in the DC link provides the initial voltage across the capacitor *C* for initial excitation of the induction generator. The resistive load is connected in parallel with the capacitor. The main objective is to ensure constant voltage across the capacitor, regardless of changes in DC load and rotor speed. This is achieved by adjusting the active and reactive power flow in the system through control of the IGBT converter switching pulses. These pulses are generated at the output of the hysteresis current controllers, as shown in Fig.3, while the reference currents are calculated within the IRFO control algorithm, as explained in Section 2.2.

2.1 Modeling of the Control System Components

2.1.1 SEIG Model

Application of vector control requires utilization of a dynamic SEIG model. Such model can be obtained by modification of the conventional dynamic model of an induction machine, as described in [10]. Here are given only the final 1st order differential equations of the conventional dynamic SEIG model in the stationary reference frame, expressed in the Laplace domain and suitable for use in MATLAB Simulink

$$si_{s\alpha} = \frac{1}{\sigma L_s L_r}(L_m^2 \omega_r i_{s\beta} - L_r R_s i_{s\alpha} + L_m \omega_r L_r i_{r\beta} + + L_m R_r i_{r\alpha} - L_r u_{s\alpha} - L_m K_{r\alpha}) \quad (1)$$

$$si_{s\beta} = \frac{1}{\sigma L_s L_r}(-L_r R_s i_{s\beta} - L_m^2 \omega_r i_{s\alpha} + L_m R_r i_{r\beta} - - L_m \omega_r L_r i_{r\alpha} - L_r u_{s\beta} - L_m K_{r\beta}) \quad (2)$$

$$si_{r\alpha} = \frac{1}{\sigma L_s L_r}(L_m R_s i_{s\alpha} - L_s \omega_r L_m i_{s\beta} - L_s \omega_r L_r i_{r\beta} - - L_s R_r i_{r\alpha} + L_m u_{s\alpha} - L_s K_{r\alpha}) \quad (3)$$

$$si_{r\beta} = \frac{1}{\sigma L_s L_r}(L_m R_s i_{s\beta} + L_s \omega_r L_m i_{s\alpha} - L_s R_r i_{r\beta} + + L_s \omega_r L_r i_{r\alpha} + L_m u_{s\beta} - L_s K_{r\beta}) \quad (4)$$

where:
$u_{s\alpha}$ and $u_{s\beta}$ are the α-axis and β-axis component of the stator voltage space-vector;
$i_{s\alpha}$ and $i_{s\beta}$ are the α-axis and β-axis component of the stator current space-vector;
$i_{r\alpha}$ and $i_{r\beta}$ are the α-axis and β-axis component of the rotor current space-vector;
R_s and R_r are the stator and rotor resistance, respectively;
L_s, L_r and L_m are the stator inductance, the rotor inductance and the magnetizing inductance, respectively;
ω_r is the rotor angular speed;
σ is the total leakage factor;
$K_{r\alpha}$ and $K_{r\beta}$ are the α-axis and β-axis component of the initially induced voltage due to the residual rotor flux linkage.

Fig.2 shows the conventional SEIG equivalent circuit described by Eqs. (1)-(4). The magnetizing flux saturation is taken into account by expressing the magnetizing inductance as a function of the magnetizing current magnitude. The corresponding characteristic can be determined from the standard no-load test, as described in [4] and [10]. The magnetizing flux saturation is, in fact, mandatory for build-up and stabilization of the SEIG's generated voltage. The iron losses of the SEIG are neglected for simplification purposes. This is justified by the fact that the emphasis is not placed on the system's efficiency or detuning analysis but rather on determining the adequate DC voltage controller.

The SEIG model shown in Fig.2 is, as such, applicable in cases when the capacitor and resistive load are connected in parallel and directly to the induction machine's stator terminals.

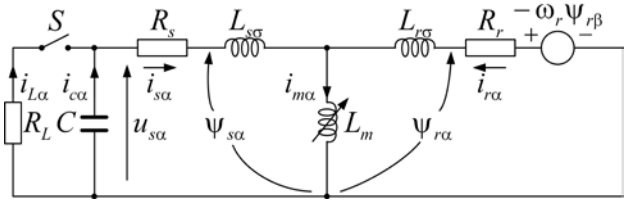

Fig.2 Conventional SEIG equivalent circuit in stationary reference frame (α-axis)

However, in the system shown in Fig.1, the IGBT converter is placed between the induction machine and the DC link so the corresponding model needs to be determined as well.

2.1.2 IGBT Converter and DC Link Models

By assuming ideal three-phase IGBT converter, the stator phase voltages and the DC-link current can be expressed in terms of the switching functions as

$$u_{sa} = \frac{1}{3}u_{dc}\left(2S_a - S_b - S_c\right) \tag{5}$$

$$u_{sb} = \frac{1}{3}u_{dc}\left(2S_b - S_c - S_a\right) \tag{6}$$

$$u_{sc} = \frac{1}{3}u_{dc}\left(2S_c - S_a - S_b\right) \tag{7}$$

$$i_{dc} = S_a i_{sa} + S_b i_{sb} + S_c i_{sc} \tag{8}$$

where u_{dc} represents the voltage across the DC-link capacitor, and i_{sa}, i_{sb} and i_{sc} represent the stator phase currents. The switching functions, S_a, S_b and S_c, are determined by the output of the hysteresis current controller in the corresponding phase.

By considering a resistive load, the DC link can be represented by the following equation:

$$u_{dc} = -\frac{1}{C}\int_0^t \left(i_{dc} + \frac{u_{dc}}{R_{dc}}\right)dt + u_{dc0} \tag{9}$$

where C is the DC-link capacitor, R_{dc} is the DC-link resistive load and u_{dc0} denotes the initial voltage across the capacitor (i.e., the battery voltage).

2.2 Control Algorithm

The IRFO control algorithm employed for control of the DC-link voltage is shown in Fig.3.

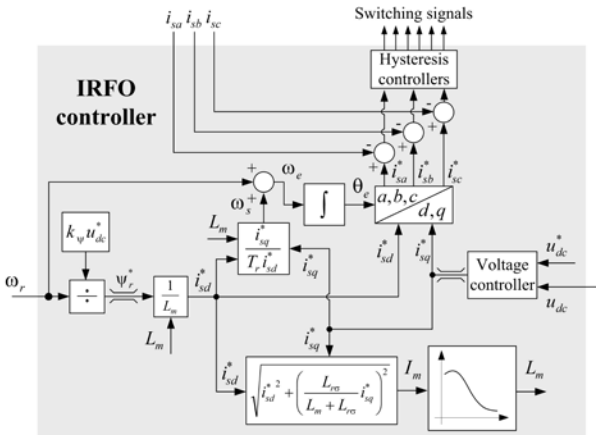

Fig.3 IRFO controller schematic diagram

In Fig.3, the reference *d*-axis component of the stator current space vector, i_{sd}^*, is responsible for magnetization, while the corresponding *q*-axis component (hereinafter: *q*-axis stator current) is responsible for torque adjustment. The equations of the proposed control algorithm are derived from the conventional SEIG model, conditions of the indirect rotor flux orientation and assumption of ideal power converter. The reference rotor flux linkage is calculated online as proportional to the ratio of the reference DC voltage and measured rotor speed. The inputs to the voltage controller are the reference and the actual DC voltage, whereas the reference *q*-axis stator current is the output variable. However, the relationship between the input and output variables of the controller is not yet defined because the adequate controller has yet to be determined.

3 PI and Fuzzy Logic Controller

3.1 PI Controller

The classical PI controller can be described by

$$y(t) = K_P\varepsilon(t) + K_I\int_0^t \varepsilon(t)dt \tag{10}$$

where $\varepsilon(t)$ represents the input error signal, in this case $\varepsilon(t) = u_{dc}^*(t) - u_{dc}(t)$, and $y(t)$ represents the output control signal, in this case $y(t) = i_{sq}^*(t)$. K_P and K_I are the proportional and integral gain of the PI controller, respectively. These gains are tunable and their optimal values can be determined by observing the PI controller response to step changes in the reference input signal as well as to various disturbances that may occur in the system, e.g. sudden changes in load. Such approach was adopted in this paper. The following optimal values were finally obtained for the PI controller parameters: K_P = 0.02 A/V and K_I = 0.2 A/Vs.

3.2 Fuzzy Logic Controllers

In this section, two different-type FL voltage controllers, i.e. Mamdani and Sugeno, are developed. Fig.4 shows the membership functions (MFs) of the Mamdani-type FL controller. In Fig.4, N, P and Z stand for *negative*, *positive* and *zero*, respectively, whereas S, M and B stand for *small*, *medium* and *big*, respectively. Hence, NS is interpreted as *small negative*. Variables *e* and *ce* represent the inputs to the FL controller, whereas *cisq* represents the output variable. Namely, *e* is the

ISBN: 978-960-474-305-6

error signal calculated as the difference between the reference and the actual DC voltage, *ce* is the change in error calculated as the difference between two consecutive values of the error signal *e*, and *cisq* is the adjustment signal for the reference *q*-axis stator current. The universe of discourse of the fuzzy variables is expressed in per unit values, which requires scaling of the input and output signals. Thus, the scaling factors equal to 0.005, 0.4 and 0.1 were chosen for *e*, *ce* and *cisq*, respectively.

The input MFs of the Sugeno-type FL controller are the same as those shown in Figs 4a and 4b. However, the output MFs are different than those shown in Fig.4c, which reflects the fact that different algorithm is used for calculation of the output variable compared to the Mamdani-type FL controller. As opposed to the triangular shaped output MFs of the Mamdani-type FL controller, the Sugeno-type FL controller has singleton output MFs defined by the following constant values: NB = -2, NM = -1, NS = -0.5, Z = 0, PS = 0.5, PM = 1 and PB = 2. As for defuzzification, for the Mamdani-type FL controller the centroid method is chosen, whereas for the Sugeno-type FL controller the weighted average method is chosen.

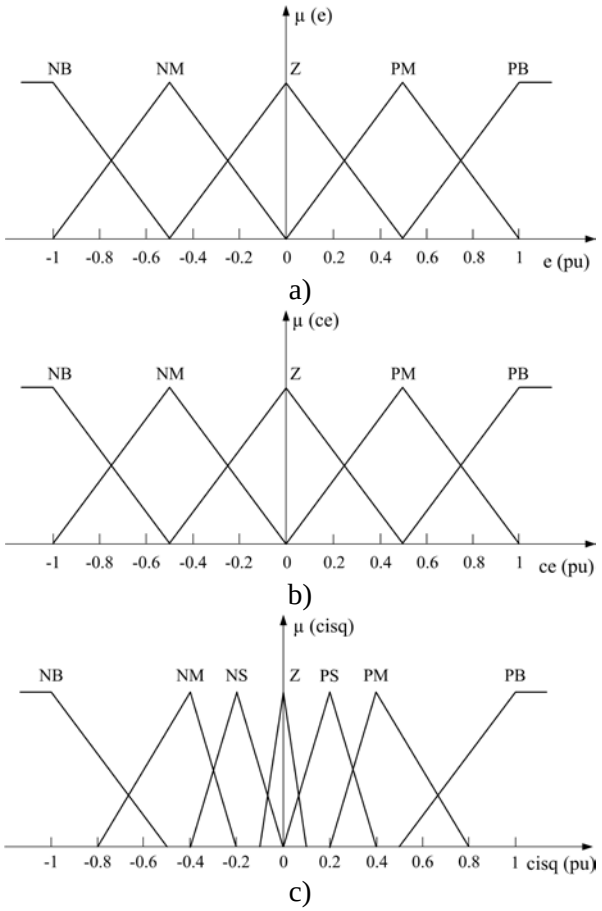

Fig.4 Membership functions of the developed Mamdani-type FL controller

The operation of the FL controllers is governed by the set of IF-THEN rules summarized in Table 1. The same set of rules applies to both FL controllers.

Table 1 Rule base for FL controllers

e / ce	NB	NM	Z	PM	PB
NB	PB	PB	PM	PS	Z
NM	PB	PM	PS	Z	NS
Z	PM	PS	Z	NS	NM
PM	PS	Z	NS	NM	NB
PB	Z	NS	NM	NB	NB

4 Results and Discussion

In this section, the performances of the optimally-tuned classical PI controller and the developed FL controllers are evaluated and compared based on the results obtained by simulations and experiments.

4.1 Simulation Results

The simulation model of the SEIG control system under consideration was built in MATLAB Simulink environment, based on the equations given in Section 2.1. To reduce the computational requirements, two different sampling times were used: T_{s1} = 1/28000 s for the induction generator, the IGBT converter and the hysteresis current controllers, and T_{s2} = 1/4000 s for the rest of the control algorithm. Parameters of the induction machine used in the analysis are given in Appendix.

In the first set of simulations (Fig.5), the load resistance was changed at t = 2 s, in a step manner, from $R_{dc} = 10^{12}$ Ω (no load) to R_{dc} = 500 Ω, while both the rotor speed and reference DC voltage were kept constant and equal to 1200 rpm and 300 V, respectively.

In the second set of simulations (Fig.6), the reference DC voltage was changed at t = 2 s, in a step manner, from u_{dc}^{*} = 250 Ω to u_{dc}^{*} = 300 Ω, while both the rotor speed and load resistance were kept constant and equal to 1200 rpm and 220 Ω, respectively.

In Fig.5a, it can be seen that the FL controllers offer about four times faster DC voltage response compared to the optimally-tuned PI controller, with about twice as low undershoot value. However, in Fig.5b, the undershoot values obtained for the FL controllers are higher compared to that of the PI controller. Still, at the expense of an increase in the undershoot value the settling time was decreased for about 0.2 s compared to the PI controller.

ISBN: 978-960-474-305-6

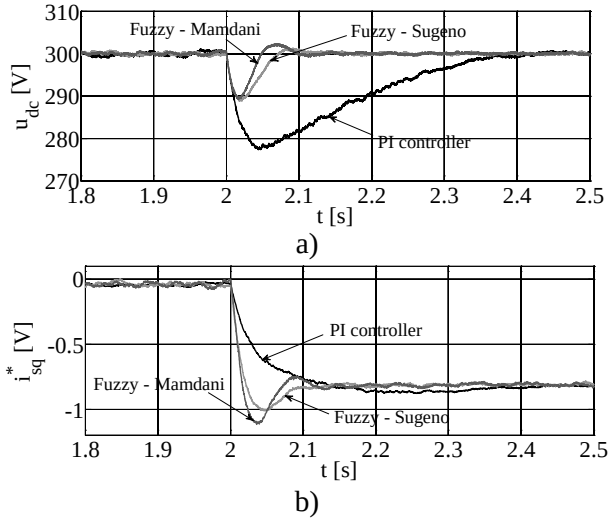

Fig.5 Simulation responses to step change in load: a) actual DC voltage and b) reference *q*-axis stator current

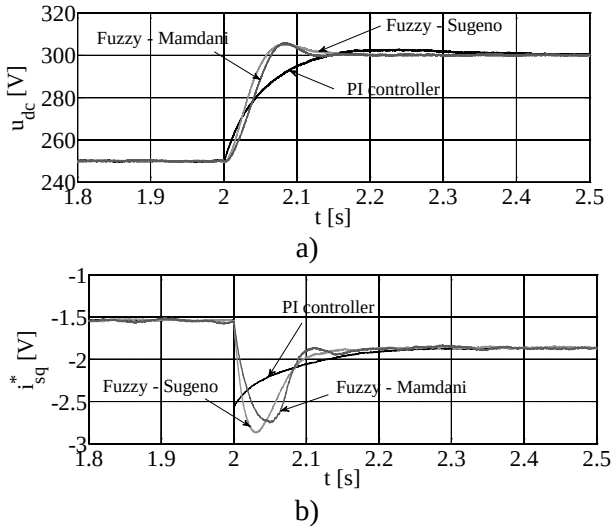

Fig.6 Simulation responses to step change in reference DC voltage: a) actual DC voltage and b) reference *q*-axis stator current

In Fig.6a, the DC voltage responses obtained for the FL controllers are again notably faster compared to the PI controller, but again at the expense of slightly higher overshoot values. Finally, in Fig.6b, it can be seen that the peak values of the reference *q*-axis stator current do not differ significantly, regardless of the controller used. However, for the FL controllers, the *q*-axis stator current derivation is significantly lower compared to the PI controller. High values of the *q*-axis stator current derivation can lead to dangerously high induced voltages in the stator windings.

The simulation results suggest that the developed FL controllers offer similar performance. In addition, their performance is significantly better compared to that of the PI controller. As for the computational requirements, they are somewhat higher for the FL controllers, especially for the Mamdani-type. In particular, when the Sugeno-type FL controller is used instead of the PI controller, the simulation execution time is extended for about 15 %. Similarly, when the Mamdani-type FL controller is used, the simulation execution time is extended for about 30 % compared to the PI controller.

4.2 Experimental Results

An experimental setup of the SEIG control system under consideration was built for experimental validation of the simulation results. The IRFO control algorithm was programed and executed in real time by using MATLAB Simulink and DS1104 R&D Controller Board, manufactured by dSPACE. The PI controller is rather easily implemented in real time due to low computational requirements. For the same reason, the Sugeno-type controller is implemented in real time more easily than the Mamdani-type controller. In fact, the developed Mamdani-type controller could not be successfully implemented in real time due to task overrun issues, which could not be resolved by reducing the number of fuzzy rules or by increasing the sampling time, while the C-code optimization was not attempted. Consequently, only the Sugeno-type FL controller was used in the experimental analysis. It should be recalled, however, that in terms of voltage control both FL controllers deliver similar results anyway.

In Figs 7 and 8, the experimental results obtained for the operating regimes described in Section 4.1 are shown.

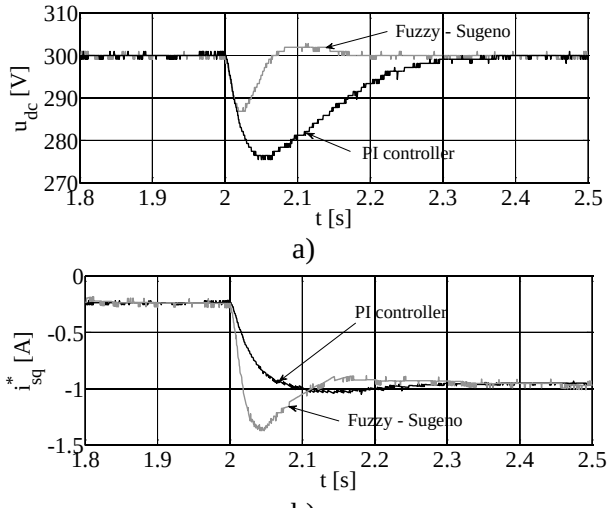

Fig.7 Experimental responses to step change in load: a) actual DC voltage and b) reference *q*-axis stator current

ISBN: 978-960-474-305-6

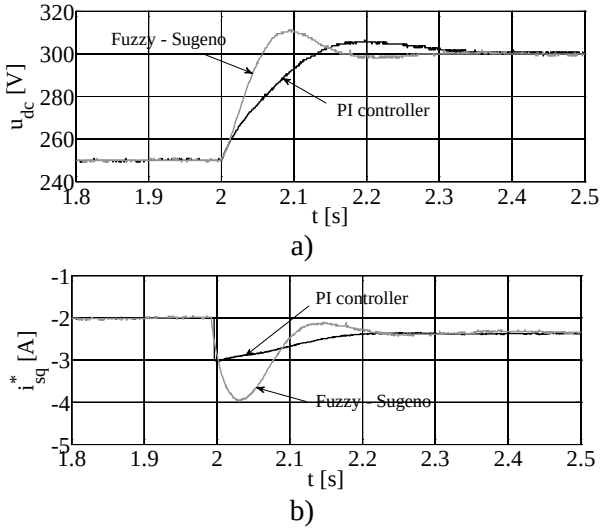

Fig.8 Experimental responses to step change in reference DC voltage: a) actual DC voltage and b) reference *q*-axis stator current

The results shown in Figs 7 and 8 are in good agreement with the simulation results shown in Figs 5 and 6, respectively. Maximum deviation between the simulation and experimental results is noted in steady state values of the reference *q*-axis stator current. This is due to the fact that in the simulation model certain losses which exist in the actual system are neglected, resulting in lower torque values and, consequently, in lower values of the reference *q*-axis stator current in simulations. These losses include mechanical losses, iron losses and stray losses of the induction machine, as well as the power converter losses. It should be noted that these deviations are independent of the type of voltage controller, while the analysis of the power losses and related phenomena is beyond the scope of this paper.

5 Conclusion

In this paper, two different-type FL voltage controllers, Mamdani and Sugeno, are developed and successfully implemented in the SEIG vector control system. Their performance is analyzed and compared with that of the classical PI controller. The obtained simulation and experimental results suggest that the FL controllers offer significantly better performance compared to the optimally-tuned PI controller, in terms of response time, settling time and robustness. However, this is achieved at the expense of an increase in the computational requirements, especially for the Mamdani-type FL controller. In future work, the performance of the developed controllers will be more thoroughly investigated and evaluated by encompassing wider ranges of rotor speeds, DC voltages and loads.

Appendix

Induction machine parameters

P_n=1.5 kW, U_n=380 V, p=2, I_n=3.81 A, n_n=1391 rpm, L_m^n =0.4058 H, $L_{s\sigma}$=0.01823 H, $L_{r\sigma}$=0.02185 H, R_s=4.293 Ω, R_r=3.866 Ω (at 20 °C), Ψ_{rn} = 0.845 Wb.

References:

[1] E. D. Basset, F. M. Potter, Capacitive Excitation for Induction Generators, *AIEE Transactions on Electrical Engineering*, Vol.54, No.5, 1935, pp. 540–545.

[2] C. Wagner, Self-excitation of Induction Motors, *AIEE Transactions on Electrical Engineering*, Vol.58, No.2, 1939, pp. 47–51.

[3] R. M. Hilloowala, A. M. Sharaf, A Rule-Based Fuzzy Logic Controller for a PWM Inverter in a Stand Alone Wind Energy Conversion Scheme, *IEEE Transactions on Industry Applications*, Vol.32, No.1, 1996, pp. 57–65.

[4] K. Idjdarene, D. Rekioua, T. Rekioua, A. Tounzi, Vector Control of Autonomous Induction Generator Taking Saturation Effect Into Account, *Energy Conversion and Management*, Vol.49, No.10, 2008, pp. 2609–2617.

[5] E. Margato, J. Faria, M. J. Resende, J. Palma, A New Control Strategy with Saturation Effect Compensation for an Autonomous Induction Generator Driven by Wide Speed Range Turbines, *Energy Conversion and Management*, Vol.52, No.5, 2011, pp. 2142–2152.

[6] Y. W. Liao, E. Levi, Modelling and Simulation of a Stand-Alone Induction Generator with Rotor Flux Oriented Control, *Electric Power Systems Research*, Vol.46, No.2, 1998, pp. 141–153.

[7] R. Leidhold, G. Garcia, M. I. Valla, Field-Oriented Controlled Induction Generator with Loss Minimization, *IEEE Transactions on Industrial Electronics*, Vol.49, No.1, 2002, pp. 147–156.

[8] D. Vukadinović, M. Bašić, A Stand-Alone Induction Generator with Improved Stator Flux Oriented Control, *Journal of Electrical Engineering*, Vol.62, No.2, 2011, pp. 65–72.

[9] J. M. Zurada, R. J. Marks, C. J. Robinson, *Computational Intelligence Imitating Life*, New York: IEEE Inc. Press, 1994.

[10] M. Bašić, D. Vukadinović, G. Petrović, Dynamic and Pole-Zero Analysis of Self-Excited Induction Generator Using a Novel Model with Iron Losses, *International Journal of Electrical Power & Energy Systems*, Vol.42, No.1, 2012, pp. 105–118.